Quantum transport in ladder-type networks: the role of nonlinearity, topology and spin

2010 J. Phys. A: Math. Theor. 43 145101

(http://iopscience.iop.org/1751-8121/43/14/145101)

J. Phys. A: Math. Theor. **43** (2010) 145101 (16pp) doi:10.1088/1751-8113/43/14/145101

Quantum transport in ladder-type networks: the role of nonlinearity, topology and spin

K Nakamura[1,2], D Matrasulov[1], U Salomov[1], G Milibaeva[1], J Yusupov[1], T Ohta[2] and M Miyamoto[2]

[1] Heat Physics Department of the Uzbek Academy of Sciences, 28 Katartal Street, 100135 Tashkent, Uzbekistan
[2] Department of Applied Physics, Osaka City University, Osaka 558-8585, Japan

E-mail: nakamura@a-phys.eng.osaka-cu.ac.jp

Received 21 August 2009, in final form 17 December 2009
Published 18 March 2010
Online at stacks.iop.org/JPhysA/43/145101

Abstract

We investigate the quantum transport of electrons, phase solitons, etc, through the mesoscopic networks of zero-dimensional quantum dots. Straight and circular ladders are chosen as networks with each coupled with three semi-infinite leads (with one incoming and the other two outgoing). Two transmission probabilities as functions of the incident energy ε show a transition from anti-phase aperiodic to degenerate periodic spectra at the critical energy ε_c which is determined by a bifurcation point of the bulk energy dispersions. TPs of the circular ladder depend only on the parity of the winding number. The introduction of a single missing bond (MB) or missing step doubles the period of the periodic spectra at $\varepsilon > \varepsilon_c$. Shift of the MB by a lattice constant results in a striking switching effect at $\varepsilon < \varepsilon_c$. In the presence of the electric-field-induced spin–orbit interaction (SOI), an obvious spin filtering occurs for the spin-unpolarized injection. For the spin-polarized injection, on the other hand, the spin transport shows spin-flip (magnetization reversal) oscillations with respect to SOI. We also show a role of soliton in the context of its transport through the ladder networks.

PACS numbers: 03.75.−b, 05.45.−a, 05.60.Gg.

1. Introduction

Recently there has been a growing interest in quantum transport in discrete physical systems characterized by networks with nontrivial topologies [1, 2]. Those networks mimic the networks of nonlinear waveguides and optical fibers [3], Bose–Einstein condensates in optical lattices [4], superconducting ladders of Josephson junctions [5], double helix of DNA, etc. In these networks, their topology and the presence of a few embedded defects are expected to play a vital role in controlling the macroscopic quantum transport such as a switching of the

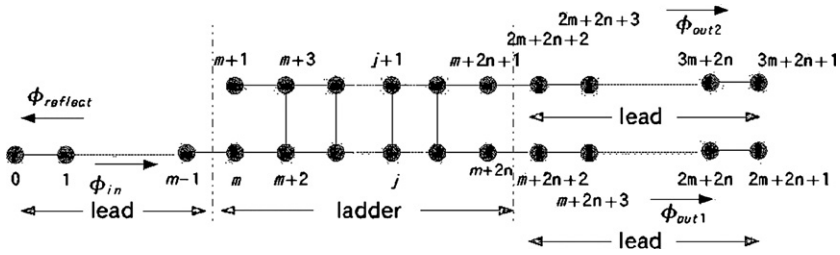

Figure 1. Straight ladder with three leads.

network current. Here, the main interest lies in the networks connecting lattice points discrete everywhere [6, 7] in contrast to another topical works on quantum graphs which are composed of connected continuous linear segments of finite length [2].

On the other hand, with the introduction of the nonlinearity to the time-dependent Schrödinger equation, the network provides a nice playground where solitons propagate in a complicated way until escaping through the attached semi-infinite leads. While nonlinear dynamics with the use of the nonlinear Schrödinger equation would not be very important in the microscopic electronic transport, it certainly plays a role in the macroscopic quantum transport [4, 5]. There already exists an accumulation of studies of the soliton propagation through the discrete chain, and its collision with small defect clusters [8]. However, little work has been done on the soliton transport through the big networks with and without defects.

In this paper we investigate the quantum transport of electrons or phase solitons through mesoscopic networks of zero-dimensional quantum dots. Typically, straight and circular ladders are chosen as model networks with each being coupled with three semi-infinite leads (with one incoming and the other two outgoing). Below we shall systematically study the following questions: (1) Is there any universal feature of quantum transport in the case of open big ladders? (2) Can a single defect bond introduced into big ladders play a crucial role in quantum transport? (3) In the context of spintronics, can open ladders which incorporate Rashba spin–orbit interaction (SOI) play a prominent role of the spin-filtering?

In section 2, based on the discrete cubic nonlinear Schrödinger equation, we examine a fate of the soliton coming from the incoming lead and propagating through the above networks in a complicated way until escaping through the three semi-infinite leads. The two transmission probabilities (TPs) based on a soliton picture are evaluated and compared with the result of Landauer formula based on the (stationary and discrete) linear Schrödinger equation. The following sections are based on the standard (linear) quantum mechanics. In section 3, TPs are explored as functions of the incident energy, and the characteristic features of the transmission spectra are found. In section 4, we shall elucidate a radical change of the transmission spectra by introducing a single defect bond into the network. The role of topology in the transport through the circular ladder is also studied in this section. Finally in section 5, the electric-field-induced SOI (i.e. Rashba interaction) is introduced to the network. Then we investigate the result of spin transport (STP) through the networks and indicate its role in magnetization oscillations and spin filtering. Summary and discussion are devoted to section 6.

2. Model networks and discrete nonlinear Schrödinger equation

As a challenge to analyze general big networks, we choose two type of networks, straight and circular ladders (see figures 1 and 2), which mimic the Josephson junction or double

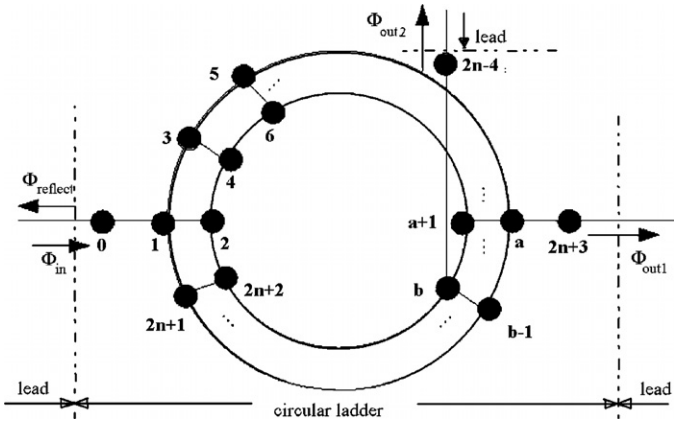

Figure 2. Circular ladder with three leads.

helix of DNA. Each system consists of an array of zero-dimensional quantum dots (i.e. lattice sites), where the central part represents a network and the external three lines stand for the attached semi-infinite leads. All lattice points are numbered in the way given in figures 1 and 2. In figure 1, for example, the incoming lead (left) is connected with the ladder at the site m and a pair of outgoing leads (right) are connected with it at the sites $m + 2n$ and $m + 2n + 1$. Suppressing three external leads, the ladder includes $2n + 2$ lattice sites and $n - 1$ steps (perpendicular to the ladder). The wavefunction comes through the incoming lead (Φ_{in}), collides with the network, and is partly reflected through the incoming lead (Φ_{ref}) and partly transmitted through two outgoing leads (Φ_{out1}, Φ_{out2}). Dynamics of a wavefunction in these open networks is described by the discrete nonlinear Schrödinger equation (DNLSE)

$$\mathrm{i}\frac{\partial \Phi_j}{\partial t} = -\frac{1}{2}\sum_l A_{j,l}\Phi_l + \Lambda|\Phi_j|^2\Phi_j, \tag{1}$$

where Λ represents the strength of cubic nonlinearity. A_{ij} is the adjacency matrix giving the topology of the network and is defined in a suitable energy unit (say, K) by

$$A_{j,l} = \begin{cases} 1 & \text{if } j \text{ and } l \text{ are linked} \\ 0 & \text{otherwise.} \end{cases} \tag{2}$$

In the case of quantum dots with a common discrete level (CDL) for each, $\Phi_j(t)$ is the wavefunction of the jth dot. The distances between linked lattice sites are fixed to a common value, say, d with d being of the order of 10–100 nm. K stands for the tunneling matrix element between connected adjacent dots. CDL is chosen around Fermi energy and prescribed to zero energy. Time t is in units of $\hbar/2K$ and $\Lambda = U/2K$ with U being the very weak Hartree term due to the electron–electron interaction. Firstly we investigate the injection of a wave packet (WP) through the incoming lead, where DNLSE governs

$$\mathrm{i}\frac{\partial \Phi_j}{\partial t} = -\frac{1}{2}(\Phi_{j-1} + \Phi_{j+1}) + \Lambda|\Phi_j|^2\Phi_j. \tag{3}$$

Consider, at $t = 0$, the Gaussian WP centered at ξ_0, with initial momentum k_0 and width γ_0. In its discrete version the time-dependent WP can be written as

$$\Phi_j(t) = \sqrt{N}\exp\left(\frac{-(j-\xi)^2}{\gamma^2} + \mathrm{i}k(j-\xi) + i\frac{\delta}{2}(j-\xi)^2\right), \tag{4}$$

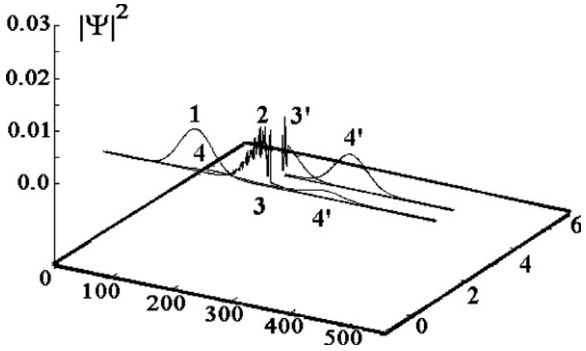

Figure 3. Soliton dynamics in the straight ladder with three leads. Time evolution of the spatial distribution of the positive wavefunction probability: $1 \to 2 \to (3, 3') \to (4, 4')$. $k = \frac{5}{8}\pi$. Basal lengths and wave number are scaled by d and d^{-1}, respectively. The schematic plot of the system 'Ladder + three leads' in the basal plane. Ladder steps are not depicted for simplicity.

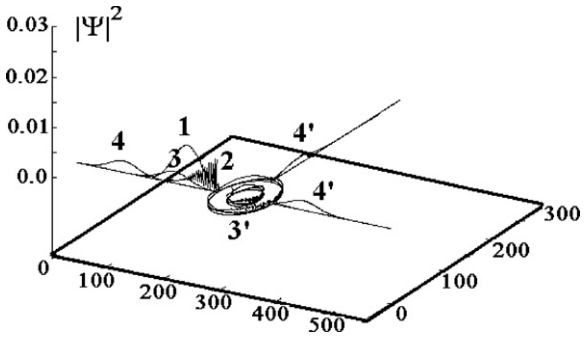

Figure 4. Soliton dynamics in the circular ladder with three leads. Time evolution of the spatial distribution of the positive wavefunction probability: $1 \to 2 \to (3, 3') \to (4, 4')$. $k = \frac{3}{5}\pi$. The same notion on lengths, wave number and ladder steps holds as in figure 3.

where $\xi(t)$ and $\gamma(t)$, which are scaled by d, are the time-dependent center of mass and width of the WP, respectively. $k(t)$ and $\delta(t)$, which are scaled by d^{-1} and d^{-2}, respectively, are the corresponding canonical-conjugate variables.

In the limit $\gamma d \gg d$, WP dynamics can be obtained from an effective Lagrangian

$$L = k\dot{\xi} - \gamma^2\frac{\delta}{8} - \frac{\Lambda}{2\sqrt{\pi\gamma^2}} + \cos(k)e^{-\eta}, \tag{5}$$

from which we have the equations of motion for ξ, k, γ and δ. In order to have a stable WP (soliton) on incoming leads it should be $\dot{\gamma} = \dot{\delta} = 0$, from which it follows that [4, 8, 9]

$$\Lambda_{\rm sol} \approx 2\sqrt{\pi}\frac{|\cos k|}{\gamma_0}. \tag{6}$$

with $\frac{\pi}{2} \leqslant k(= k_0) \leqslant \pi$ and $\delta = 0$. Under these conditions we present the numerical results of soliton dynamics colliding with a network in figures 3 and 4. The soliton propagates through the incoming lead (marked as '1'), collides with network (marked as '2'), propagates through network (marked as '3' and '3') and is partially reflected through the incoming lead (marked as '4') and partially transmitted through two outgoing leads (marked as '4'). Transmission

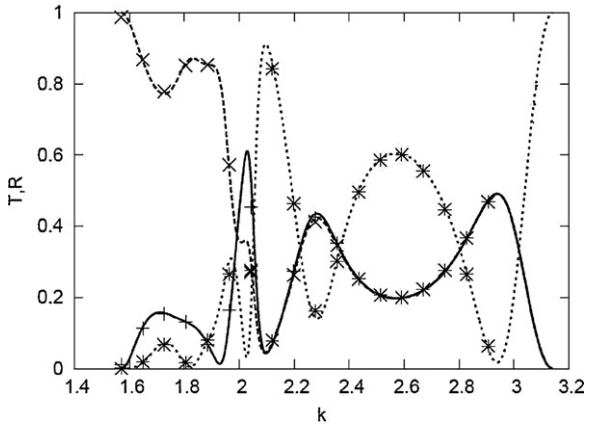

Figure 5. Comparison T_1, T_2 and R between equation (7) with use of nonlinear dynamics of a soliton and equation (11) in the Landauer formula for the time-independent linear Schrödinger equation. Number of steps in ladder is $n = 10$. The solid line and '+' for T_1, the dashed line and '$\times$' for T_2 and the dotted line and '$*$' for R. T_1 and T_2 coincides for the values of $k \geqslant k_c$, where $k_c = 2/3\pi$. Note: symbols $*$ on the solid line (which is degenerate to the dashed one) for $k \geqslant k_c$ are artifacts due to the overlap between the symbols + and $\times$.

and reflection probabilities (RP) at long enough time after collision with the network can be calculated as

$$\begin{aligned} T_1 &= \sum_{j \in \text{outgoing lead 1}} |\Phi_j|^2 \\ T_2 &= \sum_{j \in \text{outgoing lead 2}} |\Phi_j|^2 \\ R &= \sum_{j \in \text{incoming lead}} |\Phi_j|^2. \end{aligned} \tag{7}$$

The result as a function of the incident wave number k (scaled by d^{-1}) is shown in a set of symbols in figure 5 in the case of the straight ladder with number of steps $n = 10$ and length of each external lead $m = 250$. Here the initial width of the wave packet $\gamma_0 = 50$ and the initial center of mass $\xi_0 = 100$. We find that the unitarity $T_1 + T_2 + R = 1$ is always satisfied, namely no fraction of WP remains in the central network at long-enough time. We should note that the unitarity holds, irrespective of the stability or instability of solitons, i.e. whether or not the condition in equation (6) is satisfied.

Also, we compare this result with the result based on the Landauer formula [10, 11] applied to the time-independent linear Schrödinger equation for the ladder network with $N(=2n)$ lattice sites, which is connected with the semi-infinite incoming lead at '0' site and two semi-infinite outgoing leads at '$N + 1$' and '$N + 2$' sites. In the latter approach, the outgoing wavefunction $\Psi = (\Phi_0, \Phi_1, \ldots, \Phi_{N+1}, \Phi_{N+2})^T$ is determined by [12]

$$\Psi = G\Psi_{\text{in}} \tag{8}$$

for the incoming wavefunction $\Psi_{\text{in}} = (-K_s[F^{-1}(+) - F^{-1}(-)]\Phi_0(+), 0, \ldots, 0)^T$ with K_s and $F^{-1}(\pm)$ the tunneling and transfer matrices, respectively, in the leads. G is the Green's function defined by

$$G = \frac{1}{E - \tilde{H}}. \tag{9}$$

In equation (9), $\tilde{H}$ is the Hamiltonian which includes the interaction of the network with external leads [12, 13]:

$$\tilde{H} = \begin{pmatrix} \tilde{V}_0 & K_{0,1}^* & 0 & \cdots & 0 & 0 \\ K_{0,1} & & & & \vdots & \vdots \\ 0 & & H & & K_{N-1,N+1}^* & 0 \\ \vdots & & & & 0 & K_{N,N+2}^* \\ 0 & \cdots & K_{N-1,N+1} & 0 & \tilde{V}_{N+1} & 0 \\ 0 & \cdots & 0 & K_{N,N+2} & 0 & \tilde{V}_{N+2} \end{pmatrix} \tag{10}$$

where H is the unperturbed Hamiltonian. $\tilde{V}_0$, $\tilde{V}_{N+1}$, $\tilde{V}_{N+2}$ and $K_{0,1}$, $K_{N-1,N+1}$, $K_{N,N+2}$ are respectively the self-energies which renormalize the effect of semi-infinite leads and the tunneling matrices between the ladder network and leads. Noting that all tunneling matrices are unity by scaling in the present calculation, we reach the transmission T_j with $j = 1, 2$ and reflection probabilities R,

$$\begin{aligned} T_j &= |\langle N + j|G|0\rangle K_s^*[F^{-1}(+) - F^{-1}(-)]|^2 \qquad (j = 1, 2), \\ R &= |\langle 0|G|0\rangle K_s^*[F^{-1}(+) - F^{-1}(-)] - 1|^2. \end{aligned} \tag{11}$$

In figure 5 we compare the results of equation (7) with those of equation (11) in the case of the ladder with $N = 20$. Surprisingly two approaches give identical results. The reason is that the width of the WP employed here is much longer than the linear dimension of the network and that the nonlinearity plays a small role. Precisely speaking, so far as the soliton is large enough and fast enough to guarantee that the time of collision between the soliton and ladders is much shorter than the soliton dispersion time, one may resort to a linear approximation to compute the transmission coefficients [13]. In the following, therefore, we shall derive T_1, T_2 and R with the use of equation (11) applied to the linear Schrödinger equation for the ladder.

3. Transmission spectra of a straight ladder

One cannot recognize any universal feature in figure 5 in the case of a ladder with $n = 10$ steps. However, when $n \gg 10$, there appear universal characteristic features independent of n. In figure 6 transmission and reflection probabilities as a function of the energy (ε) of the incoming electron are plotted in the case of the straight ladder with $n = 50$, 100 and 200 steps. The unitarity $T_1 + T_2 + R = 1$ is always satisfied. We find the existence of a critical energy $\varepsilon_c = 0.5$ and the remarkable difference of TPs between the lower ($0 < \varepsilon < \varepsilon_c$) and higher ($\varepsilon_c < \varepsilon < 1$) energy regions. In the lower energy side, T_1 and T_2 have the anti-phase structure (i.e. T_1 takes peaks whenever T_2 has dips and vice versa), and the oscillation period decreases as $\varepsilon \to \varepsilon_c$. In the high energy side, on the other hand, two TPs are degenerate and highly periodic. All these characteristics hold irrespective of the value of n, so long as the network is large enough ($n \gg 10$). In fact, we obtained the same spectrum in the case of $n = 1000$ as in figure 6, while the oscillation period is further shortened in the latter.

The mechanism underlying the above characteristics is explained by using the perturbation theory. Let us first investigate the nature of the unperturbed long network without three leads, which can be regarded as a periodic ladder in figure 7. For a pair of upper and lower sites $2m$

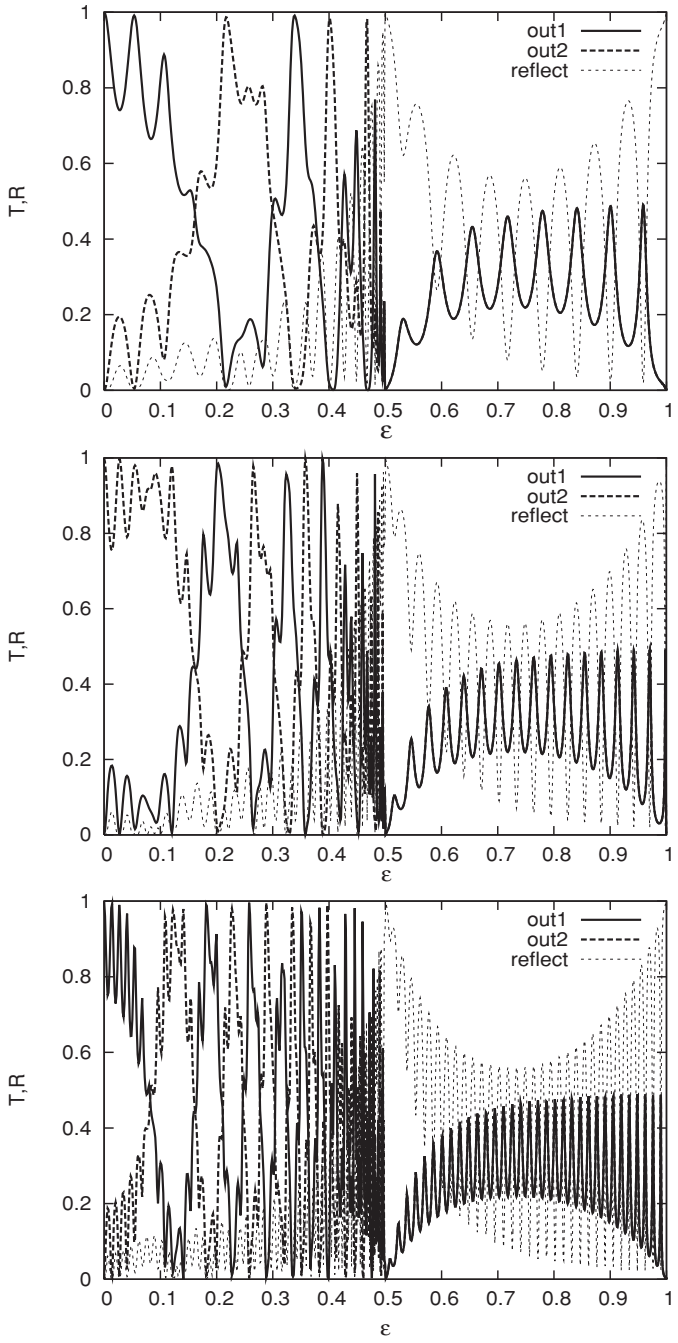

Figure 6. Transmission and reflection probabilities as functions of the energy ε. Number of steps in the ladder is $n = 50$, 100 and 200 from top to bottom panels, respectively. The solid, dashed and dotted lines correspond to T_1, T_2 and R, respectively. T_1 and T_2 are degenerate for $\varepsilon \geqslant 0.5$.

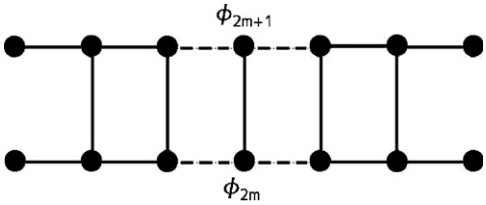

Figure 7. Unperturbed periodic straight ladder.

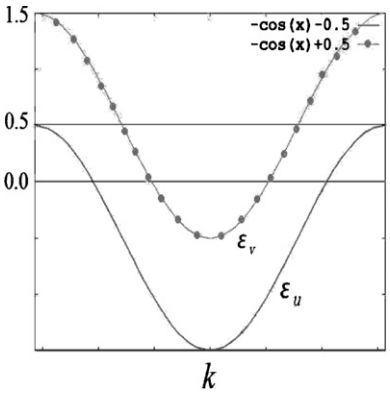

Figure 8. Two branches of energy dispersion for the unperturbed ladder. The vertical axis stands for the energy ε. ε_u: even-parity branch; ε_v: odd-parity branch.

and $2m + 1$, the wavefunctions satisfy

$$\begin{aligned} \varepsilon\Phi_{2m} &= -\tfrac{1}{2}(\Phi_{2(m+1)} + \Phi_{2(m-1)} + \Phi_{2m+1}), \\ \varepsilon\Phi_{2m+1} &= -\tfrac{1}{2}(\Phi_{2(m+1)+1} + \Phi_{2(m-1)+1} + \Phi_{2m}). \end{aligned} \tag{12}$$

Let us introduce the new basis functions u_m and v_m with the use of the transformation:

$$\begin{cases} u_m = \frac{1}{\sqrt{2}}(\Phi_{2m} + \Phi_{2m+1}) \\ v_m = \frac{1}{\sqrt{2}}(\Phi_{2m} - \Phi_{2m+1}). \end{cases} \tag{13}$$

u_m and v_m stand for the even- and odd-parity states in each step, respectively. Using this new basis, the eigenvalue problem is decoupled, namely, reduced to the even- and odd-parity parts. Assuming $u_m \sim \mathrm{e}^{\mathrm{i}km}$ and $v_m \sim \mathrm{e}^{\mathrm{i}km}$ for an infinitely long ladder, we find eigenvalues

$$\varepsilon_u = -\cos(k) - \tfrac{1}{2} \qquad \varepsilon_v = -\cos(k) + \tfrac{1}{2}. \tag{14}$$

The even-parity branch ε_u and odd-parity one ε_v constitute a pair of energy bands (see figure 8). It should be noted that while for $0 \leqslant \varepsilon \leqslant \varepsilon_c$, both energy branches ε_u and ε_v appear, only the ε_v branch can survive for $\varepsilon \geqslant \varepsilon_c$.

In the presence of the perturbation, namely, in the case of the ladder attached with three leads in figure 1, $u_m, v_m \sim \mathrm{e}^{\mathrm{i}km}$ are no longer the eigenstates: the mixing (superposition) of states occur within the odd-parity manifold only for $\varepsilon \geqslant \varepsilon_c$ and between the odd- and even-parity manifolds for $0 \leqslant \varepsilon \leqslant \varepsilon_c$. In the case of $\varepsilon \geqslant \varepsilon_c$, therefore, the wavefunction retains the same feature as the unperturbed state: the coefficients of the wavefunction Φ_{2m} and Φ_{2m+1} have the identical magnitude. This fact holds at the ladder edge with $m = 2n$ and

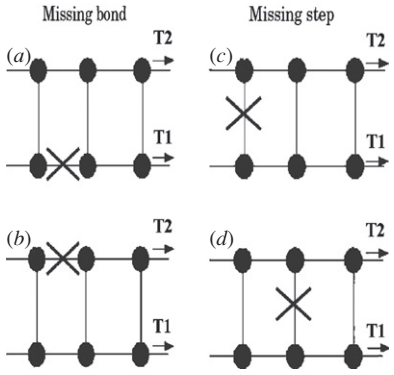

Figure 9. Missing bonds (A, B) and missing steps (C, D). Each figure shows only six quantum dots in the midst of the long regular ladder. $A(B)$ corresponds the case that a single bond with $\times$, which is parallel to the ladder, is missing. Missing bond in (B) is displaced upward from one in (A) by a lattice constant; $C(D)$ corresponds the case that a single step with $\times$, which is perpendicular to the ladder, is missing. Missing step in (D) is displaced to right from one in (C) by a lattice constant.

$m = 2n + 1$ as well. Consequently, we see the degeneracy of oscillations for T_1 and T_2 in figure 6. On the other hand, in the case of $0 \leqslant \varepsilon \leqslant \varepsilon_c$, we see the superposition of u_m and v_m:

$$\alpha u_m + \beta v_m = \tfrac{1}{\sqrt{2}}(\alpha + \beta)\Phi_{2m} + \tfrac{1}{\sqrt{2}}(\alpha - \beta)\Phi_{2m+1}. \tag{15}$$

As a result, wherever the coefficient of Φ_{2m} has a big magnitude, that of Φ_{2m+1} has a small one, and vice versa. This is true even at the ladder edge, explaining the anti-phase oscillation for T_1 and T_2 in figure 6.

Thus, the transmission spectra of the straight ladder attached with three leads show a mixing between different parity states and an anti-phase structure in the output in the lower energy regime ($0 \leqslant \varepsilon \leqslant \varepsilon_c$), while, in the higher energy regime ($\varepsilon_c \leqslant \varepsilon \leqslant 1$), no mixing and the degenerate periodic structure are seen in the output.

4. Role of defect bonds and topology

One of the most essential questions of quantum networks is whether or not only a single defect bond introduced into big networks will play a crucial role in quantum transport. Now we proceed to investigate the influence of a missing bond (MB) embedded in the midst of the ladder network with $N = 100$ steps on the quantum transport. The left and right panels in figure 9 correspond to breaking a bond and step, which are parallel and perpendicular to the ladder, respectively. The corresponding transmission spectra are given in figures 10 and 11. Consider the case with a MB in the mid-ladder. For $\varepsilon > \varepsilon_c$, the regular oscillation of T_1 and T_2 retains the degeneracy and in-phase structure, but has a period twice as large as the one without MB. For $\varepsilon < \varepsilon_c$, T_1 shows a radical change from the complete transmission ($T_1 = 1$) to the complete reflection ($T_1 = 0$) and vice versa when the MB moves by a lattice constant, which can be taken as a switching effect (see figure 10). The issue of a missing step (MS) in the midst of the ladder is as follows: for $\varepsilon > \varepsilon_c$, besides the period-doubling phenomenon, the regular oscillation shows a phase shift by half a period when the MS moves by lattice constant (see figure 11). We should note that so long as a reference MB or MS is embedded in the midst of big networks, the above discoveries (i.e. period doubling and phase shift for $\varepsilon > \varepsilon_c$,

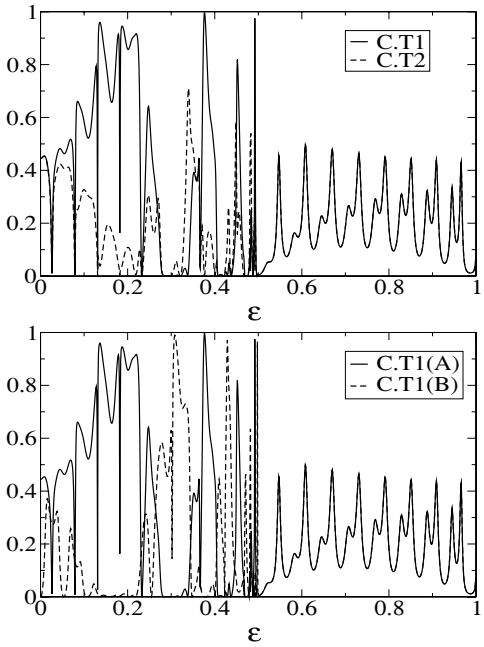

Figure 10. Transmission probabilities as functions of energy ε in the case of a single missing bond (MB). Numbers of steps (n) and of lattice points in the ladder are 100 and 200, respectively. The upper panel includes T_1 (solid line) and T_2 (dashed line) in the case where the MB lies between lattice points 100 and 102 (: case 'A' in figure 9). The lower panel includes only T_1, and the solid and dashed lines correspond to cases 'A' and 'B' in figure 9, respectively. Spectra are degenerate for $\varepsilon \geqslant 0.5$.

and the switching effect for $\varepsilon < \varepsilon_c$) remain unchanged, irrespective of the absolute location of such a defect bond in figure 9. Thus, an introduction of a single MB or MS into a big network results in a radical change in the transmission spectra.

In order to see the role of another topology of networks we consider the annular circular ladder and investigate the twist effect (see figure 12) on quantum transport (see figure 13).

In the case of no twist, the spectra show the same remarkable transition when ε crosses $\varepsilon_c = 0.5$ as in the case of the straight ladder. We find that in the lower energy side, T_1 and T_2 have the anti-phase structure, and the oscillation period decreases as $\varepsilon \to \varepsilon_c$. In the high energy side, on the other hand, two TPs are degenerate and highly periodic. In the presence of a single twist (i.e. analog of Möbius strip) the spectra again show a remarkable transition at $\varepsilon_c = 0.5$, but the detailed feature differs from the result for the no twist case. See the great reduction of T_1 and T_2 in the lower energy region in the single twist case. On the other hand, in the double twists case the result is identical to that of no twist case. The spectra are determined by the parity of the winding number (WN). The winding of the circular ladder is identical to the application of an Aharonov–Bohm flux with the WN multiplied by a half of the flux quantum $\frac{\phi_0}{2} = \frac{hc}{2e}$. Thus the topology of networks plays a vital role in quantum transport.

5. Spin–orbit interaction and spin transport

Recent progress in semiconductor spintronics revealed a way of controlling the magnetization of devices not by a magnetic but by an electric field. The idea is to use the Rashba SOI

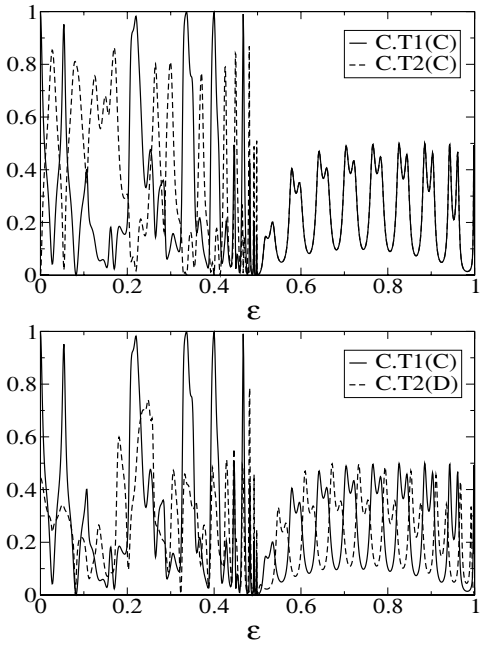

Figure 11. The same as figure 10 but in the case of a single missing step (MS). The upper panel includes T_1 (solid line) and T_2 (dashed line) in the case where the MS lies between lattice points 100 and 101 (: case 'C' in figure 9). The lower panel includes only T_1, and the solid and dashed lines correspond to cases 'C' and 'D' in figure 9, respectively.

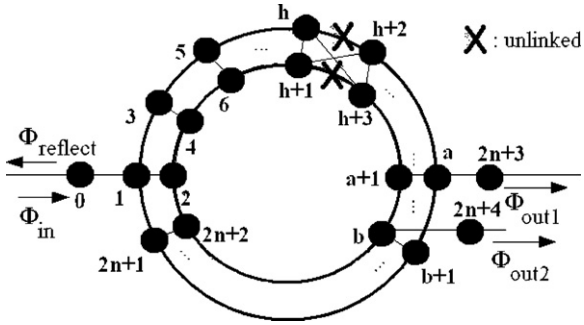

Figure 12. Twisted annular circle. '×' means the disconnection, $h+1$ and $h+2$ (likewise, h and $h+3$) are connected.

[14–17] whose strength is tuned by the external gate voltage. In this section, by introducing the SOI into the network, we investigate STP (spin-dependent transport) as well as charge transport (CTP). According to the pioneering work of Datta and Das [11, 18, 19], we first consider the STP for the spin-polarized injection. The network Hamiltonian generalized so as to include the Rashba SOI is given by

$$-\frac{1}{2}\sum_{l} A_{j,l}\Phi_l + \alpha(\sigma \times p)_z \Phi_j = \varepsilon \Phi_j, \tag{16}$$

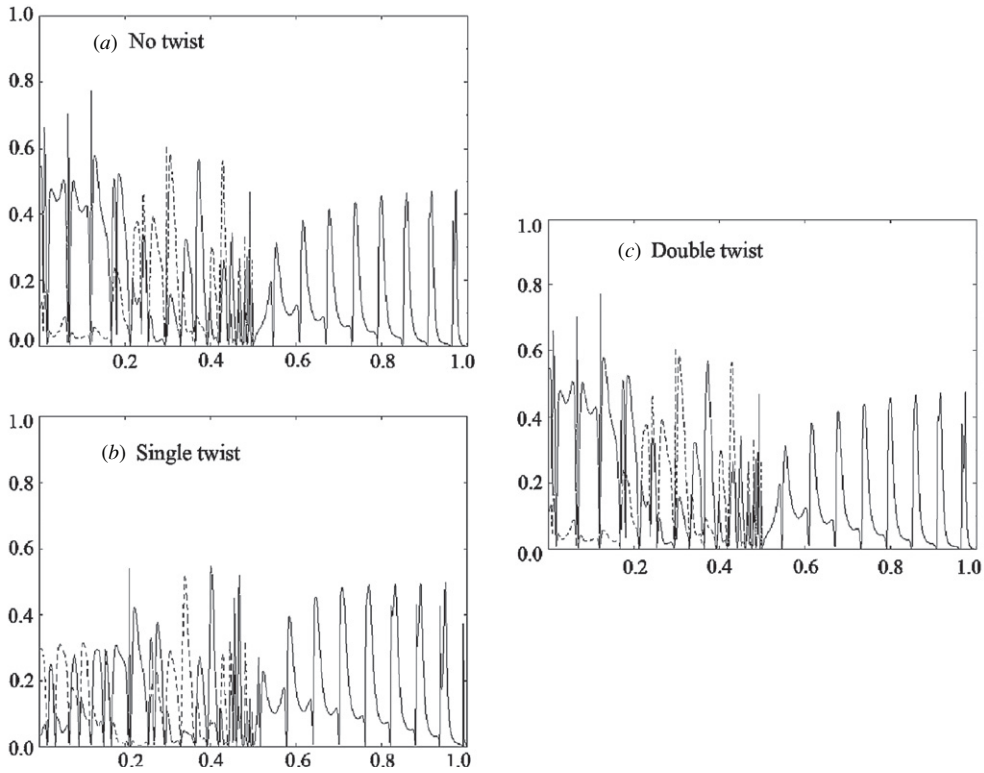

Figure 13. Transmission probabilities as functions of the energy ε (solid for T_1 and dashed for T_2). Three cases of twisted circles: (a) no twist; (b) a single twist and (c) double twists. Spectra are degenerate for $\varepsilon > \varepsilon_c$, though no bold line appears.

with $\Phi_j \equiv (\phi_{j,\uparrow}, \phi_{j,\downarrow})^T$ the two component wavefunction, $\alpha = -\frac{e\hbar}{4m^2c^2K} E_z$ the strength of the Rashba SOI in the case of an vertically applied electric field and σ stands for Pauli matrices. In equation (16), energy is scaled by the tunneling matrix element K. For convenience in our numerical calculation, we introduced dual ladders to assign each of them to up- and down-spin states, respectively (see figure 14). The STP is quantified as $T_{1,2}^{\text{spin}} = T_{1,2}(\uparrow) - T_{1,2}(\downarrow)$ and the CTP as $T_{1,2}^{\text{charge}} = T_{1,2}(\uparrow) + T_{1,2}(\downarrow)$.

In figure 15 the STP as functions of energy is plotted for different values of the strength of the Rashba SOI α. We consider the spin-polarized $\left(S_z = +\frac{1}{2}\right)$ injection. In the absence of spin–orbit interaction the STP T_1^{spin}, T_2^{spin} as functions of ε show the same spectra as in the case of CTP T_1, T_2 (see figure 6), because we have no contribution from $T_{1,2}(\downarrow)$. Against the variation of SOI, the STP shows spin-flip (magnetization reversal) oscillations (see figure 15), while keeping the anti-phase structure of T_1^{spin} and T_2^{spin} in the range $\varepsilon < \varepsilon_c(=0.5)$. Against the variation of SOI, by contrast, the CTP keeps the spectral feature without SOI (see figure 6).

Finally we shall investigate the most interesting subject, namely the STP in network systems with SOI for the injection of the spin-unpolarized electron. Figure 16 shows T_1^{spin} and T_2^{spin} as functions of ε for non-zero values of α. Astonishingly we find $T_1^{\text{spin}} = -T_2^{\text{spin}}$ for any value of ε in the case of $\alpha \neq 0$. This discovery indicates that a straight ladder with three leads plays a role of the spin filtering, i.e. the unpolarized electron is decomposed into mostly

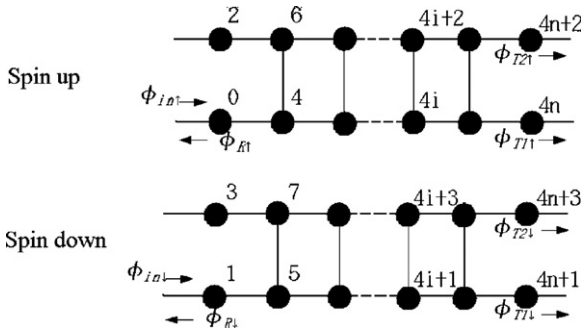

Figure 14. Spinor ladders. For computational purpose, dual ladders are introduced with each corresponding to spin-up and spin-down states.

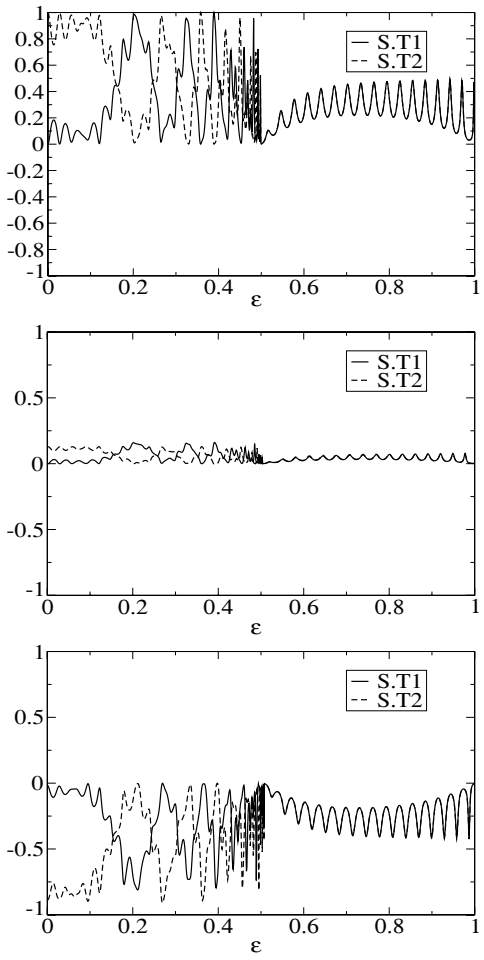

Figure 15. Spin transport T_1^{spin} (solid) and T_2^{spin} (dashed) for different values of spin–orbit interaction in the case of spin-polarized injection. The panels from top to bottom correspond to $\alpha = 0.0$, 0.12 and 0.18, respectively.

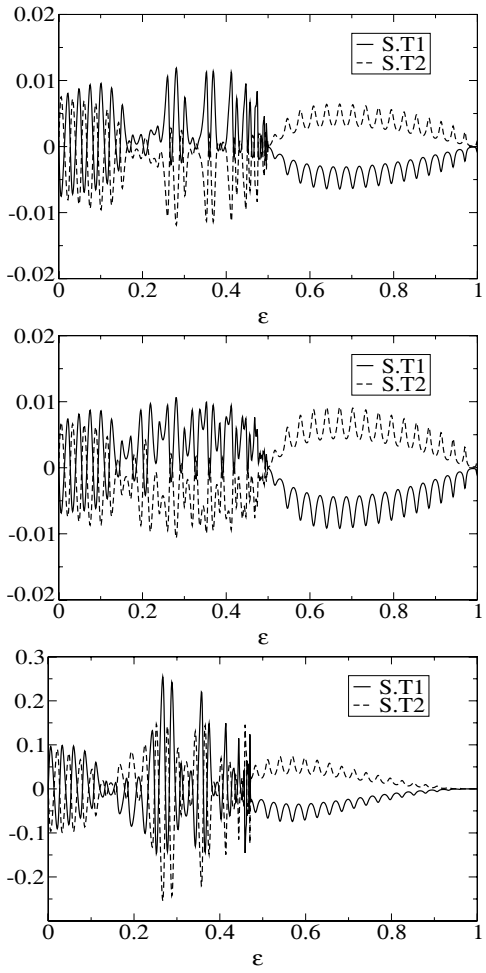

Figure 16. The same spin transport T_1^{spin} (solid) and T_2^{spin} (dashed) as in figure 12, but in the case of spin-unpolarized injection. The panels from top to bottom correspond to $\alpha = 0.1, 0.12$ and 0.46, respectively.

spin-up and mostly spin-down components through its transport in the ladder. In the context of nanoscience, this is the most essential issue among many other discoveries in the present work.

6. Summary and discussions

Choosing straight and circular ladders as large network models and attaching them with one incoming and two outgoing semi-infinite leads, we examined the quantum transport of an electron or phase soliton. In the beginning, by adding a small cubic nonlinearity (e.g. Hartree term) to the discrete time-dependent linear Schrödinger equation, we showed how the incoming soliton bifurcates at the entrance of the ladder-type network and is ultimately evacuated from the network through three leads.

We chose a soliton large enough and fast enough to guarantee the time of collision between the soliton and ladders to be much shorter than the soliton dispersion time. On the basis of this soliton picture, two transmission probabilities ($T_{1,2}$) and a reflection probability (R) were evaluated, which proved to accord with the corresponding probabilities obtained from the linear methodology, i.e. Landauer formula applied to the time-independent linear Schrödinger equation. The main part of the paper was then devoted to the results of the latter (linear) methodology. Firstly we investigated T_1, T_2 as functions of the energy ε of the incident electron. Both probabilities show a transition from anti-phase aperiodic to degenerate periodic spectra at the critical energy $\varepsilon_c = 0.5$, whose value is determined by a bifurcation point of the bulk energy dispersions. TPs of the circular ladder depend only on the parity of the WN, because the WN plays a role of an Aharonov–Bohm flux with its magnitude being a half of flux quantum multiplied by the WN.

The introduction of a single defect bond into big networks radically changes the macroscopic transport spectra. A MB parallel to the ladder in the network doubles period of the periodic spectra for $\varepsilon > \varepsilon_c$. For $\varepsilon < \varepsilon_c$, the shift of a single MB by a lattice constant results in the switching between two outgoing leads. An MS leads to a phase shift besides the period doubling for $\varepsilon > \varepsilon_c$.

Finally, by introducing the electric-field-induced Rashba SOI, we explored the STP $\left(T_1^{\text{spin}}, T_2^{\text{spin}}\right)$ for the spin-polarized injection. At zero SOI, T_1^{spin} and T_2^{spin} as functions of ε show the same spectra as in the case of CTP. Against a variation of SOI, however, this structure shows a coherent spin-flip (magnetization reversal) oscillations. On the other hand, the injection of the spin-unpolarized electron leads to the spin filtering, namely, the unpolarized electron is decomposed spatially into mostly spin-up and mostly spin-down components through its transport in the ladder. Therefore the present network can be used as a spin-filtering device. This is the most striking issue of this paper. The present results would also be applicable to the propagation of a wide-enough soliton in Josephson junction networks and of a wave packet in Bose–Einstein condensates in optical-lattice networks, although the linear and static approximation will break down and the transport would be highly nonlinear and more generic.

Acknowledgments

We are grateful for the valuable discussions with A Terai, Y S Kivshar, B Abdullaev, and F Abdullaev. The work is partly supported through a project of the Uzbek Academy of Sciences (FA-F2-084).

References

[1] Harary F 1969 *Graph Theory* (Reading, MA: Addison-Wesley)
[2] Kottos T and Smilansky U 1997 *Phys. Rev. Lett.* **79** 4794
Kottos T and Smilansky U 1999 *Ann. Phys. (NY)* **274** 76
[3] Kivshar Y S and Agarwal G P 2003 *Optical Solitons: From Fibers to Photonic Crystals* (San Diego: Academic)
[4] Trombettoni A and Smerzi A 2001 *Phys. Rev. Lett.* **86** 2353
[5] Binder P *et al* 2000 *Phys. Rev. Lett.* **84** 745
Burioni R *et al* 2000 *Europhys. Lett.* **52** 251
[6] Flach S and Willis C R 1998 *Phys. Rep.* **295** 181
[7] Ablowitz M J, Prinari B and Trubatch A D 2004 *Discrete and Continuous Nonlinear Schrödinger Systems* (Cambridge: Cambridge University Press)
[8] Burioni R, Cassi D, Sodano P, Trombettoni A and Vezzani A 2005 *Chaos* **15** 043501
Burioni R, Cassi D, Sodano P, Trombettoni A and Vezzani A 2006 *Physica* D **216** 71
[9] Malomed B A and Weinstein M I 1996 *Phys. Lett.* A **220** 91

[10] Buttiker M, Imry Y, Landauer R and Pinhas S 1985 *Phys. Rev.* B **31** 6207
[11] Datta S 1995 *Electronic Transport in Mesoscopic Systems* (Cambridge: Cambridge University Press)
[12] Ando T 1991 *Phys. Rev.* B **44** 8017
[13] Miroshnichenko A F, Flach S and Malomed B A 2003 *Chaos* **13** 874
[14] Rashba E I 1960 *Fiz. Tverd. Tela (Leningrad)* **2** 1224
Rashba E I 1960 *Solid State Ionics* **2** 1109 (Engl. Transl.)
[15] Bychkov Y A and Rashba E I 1984 *J. Phys. C: Solid State Phys.* **17** 6039
[16] Souma S and Nikolic B K 2005 *Phys. Rev. Lett.* **94** 106602
[17] Nikolic B K, Souma S, Zarbo L P and Sinova J 2005 *Phys. Rev. Lett.* **95** 046601
[18] Datta S and Das B 1990 *Appl. Phys. Lett.* **56** 665
[19] Zutic I, Fabian J and Sarma S Das 2004 *Rev. Mod. Phys.* **76** 323